

Static ductility evaluation of corroded steel plates considering surface roughness characteristics

*Naftary Gathimba¹⁾ and Yasuo Kitane²⁾

^{1), 2)} *Department of Civil and Environmental Engineering, Nagoya University, Nagoya
464-8603, Japan*

¹⁾ gathimba.naftary.kimenju@i.mbox.nagoya-u.ac.jp

ABSTRACT

In this paper, thickness data obtained from corroded steel pipes piles, which had been exposed to the marine environment for 19.5 years, were used to construct finite element (FE) models of corroded coupons. A nonlinear FE analysis to simulate tensile coupon tests was conducted on these models using a general-purpose FE analysis software. In addition, different surface roughness parameters of the corroded coupons were determined as specified in ISO 25178-2. Surface roughness due to corrosion was found to cause stress concentration and strain localization during loading which in turn led to a reduction in ductility. The variations between the surface roughness characteristics and ductility are discussed in this paper.

1. INTRODUCTION

In Japan, many marine steel structures, which were constructed during the high economic growth period in the 1960s, have been severely degraded by corrosion (Suzuki 2008). Corrosion leads to surface roughness and reduction in plate thickness (Garbatov 2014). Many studies have been undertaken to determine the residual capacity of corroded steel structures in order to apply appropriate retrofitting methods. However, most studies have focused only on residual strength of corroded steel members. Ahmmad (2010) studied deformability as the ratio of total elongation of pitted steel plates to uncorroded plates. From their research, clear dependence of elongation was shown with respect to the surface configuration such as the minimum cross-sectional area of the specimens, the maximum depth of the pit cusp from the mean corrosion diminution level, and pitting patterns. They proposed empirical formulae for the reduction of deformability and the reduction of energy absorption of pitted plates. Qin (2016) studied the contribution of surface roughness to degradation of mechanical properties of steel, and found a significant decrease in the ductility after corrosion rate exceeded 15%, where corrosion rate was defined as mass loss percentage due to

¹⁾ Graduate Student

²⁾ Associate Professor, PhD

corrosion. However, no detailed investigation was conducted concerning this observation.

The objective of the current study is to investigate the significance of surface roughness on ductility behaviour of corroded steel plates. Due to unevenness on the surface of corroded steel members, it is anticipated that during load application high-stress concentration will be experienced, resulting in strain localization which will cause a reduction in ductility. To this end, elastoplastic nonlinear large deformation analysis of corroded and uncorroded coupon specimens subject to static monotonic tension is presented in this paper. Eight-node solid brick elements (C3D8) and elastoplastic material behaviour are employed while conducting the FE analysis using Abaqus software (Simulia, 2014). Corrosion modelling is done using measured data from corroded steel pipe piles. Furthermore, using the measured surface heights data, the condition of the surface is studied by computing different surface roughness parameters using codes written in MatLab (Mathworks, 2018). Strain distribution on the analyzed models is used to study the ductility behaviour of the corroded specimens. Finally, relationships between ductility and surface roughness parameters are discussed.

2. THICKNESS DATA OF CORRODED PIPE PILES

Thickness data for corrosion modelling in the current study was obtained from previous measurements from corroded steel pipe piles (Tamura 2005). The pipe piles had been under marine exposure at Nippon Steel Kimitsu Steelworks for about 19.5 years. The condition of exposure is shown in Fig. 1. The pipes' nominal outer diameter, nominal thickness, and lengths in the initial condition measured 406.4 mm, 9 mm, and 10 m, respectively. The pipe piles are spiral pipes of steel type SKK490. After 19.5 years of exposure, the pipes were cut into pieces of 1200 mm in length.

Previous studies have shown that corrosion under marine environment proceeds at different rates at different exposure zones whereby thickness reduction is greatest at the splash zone (JSCE 2009). The alternate drying and wetting cycles caused by the action of the splashes at this zone facilitates corrosion more than other zones. As a result, corroded surfaces exposed in the splash zone are expected to exhibit severer corrosion and rougher corrosion surfaces, which are considered very suitable for the objective of this study. Therefore, the pipe section used in the current study was selected at an elevation of between +2700 mm and +3900 mm from the mean sea level (MSL) representing the splash zone.

Thickness measurement employed two laser displacement meters where one was positioned on the outside and another one on the inside of the pipe to obtain the surface profile data of both the inside and outside of the pipe and consequently obtain the remaining thickness. Thickness measurements were made at 1 mm interval in the vertical direction and 1.04 mm in the circumferential direction. Fig. 2 shows the experimental set-up for thickness measurement. Surface thickness data, $Z(x,y)$, was obtained as a 1201 by 1200 matrix for each piece of pipe. Fig. 3 shows a contour plot of the remaining thickness distribution on an opened-up pipe surface. The corresponding thickness statistics are also shown in the figure. The diagonal lines in Fig. 3 represent the weld bead. Such areas were avoided when selecting data for

corrosion modelling. Using the initial pipe thickness value of 9 mm, the average loss in thickness was calculated, and used as a measure of the degree of degradation due to corrosion.

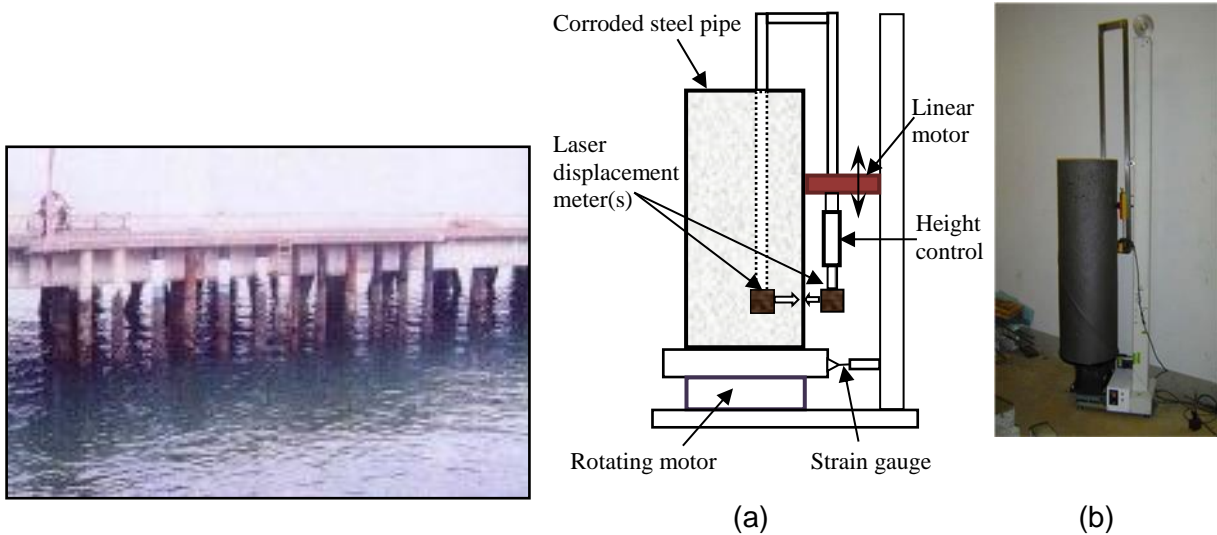


Fig. 1. Exposure test condition of the steel pipe piles (Tamura 2005)

Fig. 2. Thickness measurement: (a) schematic diagram (b) pictorial presentation (Tamura 2005)

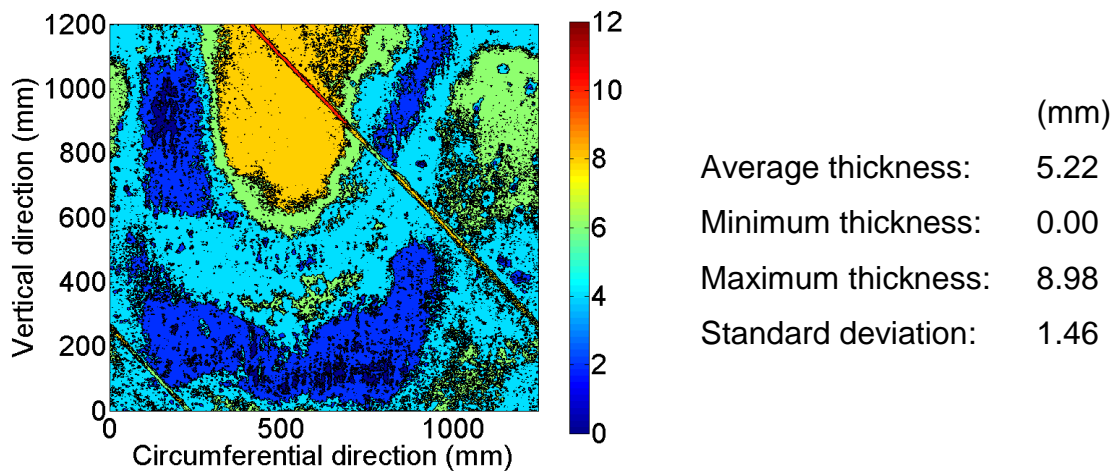


Fig. 3 Remaining thickness details for the pipe exposed at the splash zone of the marine environment

3. FINITE ELEMENT ANALYSIS

Measured thickness data was used to model only the mid-section of the standard JIS No. 5 tensile coupon specimen (JIS 2011). The tapered section together with the grip ends was left uncorroded. The modelled corroded section measured 90 mm by 24.96 mm. Corrosion surface was modelled only on one side of the specimen by

assuming insignificant corrosion inside the pipe. Different models were prepared by selecting thickness data at different locations of the pipe as shown in Fig. 4. For consistency in thickness data selection, the whole pipe surface was subdivided into 100 x 100 mm areas resulting in a grid of 12 x 12 (=144) units. Each area was then labelled according to its relative position in the grid, i.e. $A_j - i$, where j and i are position indices in the vertical and circumferential directions, respectively. Corrosion data for different coupons were selected from within these segmented areas and the resultant coupon labelled accordingly. For instance, the first coupon selected from area A1-1, would be labelled as A1-1-S1. Using 8-node brick elements (C3D8) and elastoplastic material behaviour, finite element (FE) model of corroded steel coupons was constructed in a general purpose finite element software, Abaqus (Simulia 2014), as shown in Fig. 4(b). Basic material properties obtained from previous material testing were employed in this FE analysis, and they are summarized in Table 1. Swift power-law strain hardening model (Wang 2015) was used to construct an extended material model until failure. The full true stress-plastic strain material model used in this study is shown in Fig. 4(c). Loading was applied as a displacement on one end of the coupon in simulating monotonic loading conditions for the tensile tests.

Table 1 Basic material properties of SKK steel

Poisson's ratio, ν	Young's modulus, E , (GPa)	Yield strength, σ_y (MPa)	Tensile strength, σ_u (MPa)
0.283	203	362	394

4. Results and discussions

4.1 Surface roughness characteristics

Surface analysis was conducted for each coupon in the region within the gauge length, i.e. a 50 mm by 24.96 mm area. In order to obtain the roughness surface from the surface profile due to corrosion, nominal form, an attribute of the general shape of the specimen was removed through least squares mean plane fitting. After obtaining

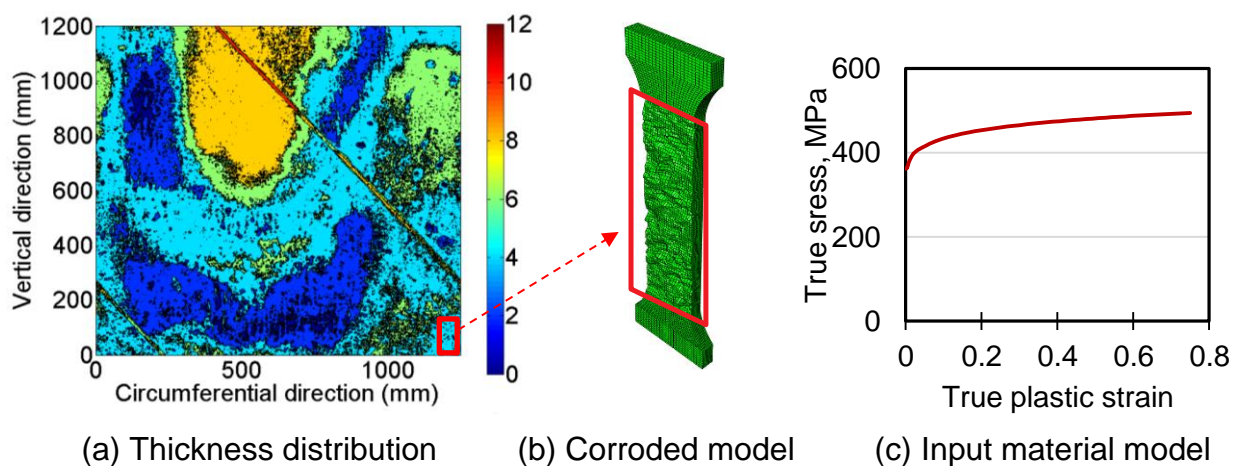


Fig. 4 Corrosion modelling

the roughness surface, surface roughness parameters, specified by ISO 25178 (2012) were then calculated. Roughness parameters calculated in this study are the maximum surface height, S_z , the average surface height, S_a , the root mean square gradient, S_dq and the developed interfacial area ratio, S_dq . Definitions of these parameters are summarized in Table 2. Calculated roughness parameters of representative corroded coupon models are shown in Table 3 together with some basic statistical characteristics of the remaining thickness, i.e. minimum (t_{min}), maximum (t_{max}), mean (t_{mean}), standard deviation (t_{std}) and coefficient of variation (COV) values.

Thickness loss values vary between 0.3 and 6.7 mm, which translates to 4.2% to 73.9% of the initial thickness of 9 mm. Thus, the selected models presented here represent a wide spectrum of corrosion degradation, from mild to severe corrosion. A closer examination of the height roughness parameters reveals a strong correlation with degree of degradation where the values increase with an increase in corrosion degradation. In the case of severe corrosion degradation, more than 50% increment of surface area due to surface roughness can be attained as seen in model A2-5-S2.

Table 2 List of roughness parameters calculated in this study

Parameter name	Expression	Attribute	Remarks
(1) Maximum Surface height	$Sz = Sp + Sv = Sp - Sv$	Height characteristic	Sp, Sv is the maximum peak and valley heights respectively
(2) Average surface height	$Sa = \frac{1}{n_x n_y} \sum_{j=1}^{n_y} \sum_{i=1}^{n_x} \eta(x_i, y_j) $	Height characteristic	$\eta(x_i, y_j)$, is the roughness data matrix of size n_x by n_y
(3) Root mean square gradient	$Sdq = \sqrt{\frac{1}{A} \sum_{j=2}^{n_y} \sum_{i=2}^{n_x} \rho_{ij}^2}$	Hybrid characteristic	ρ_{ij}^2 is the surface slope at a point, A is the planar surface area representing uncorroded surface
(4) Developed interfacial area ratio	$Sdr = \frac{1}{A} \left(\sum_{y=1}^{n_y-1} \sum_{x=1}^{n_x-1} A_{ij} - A \right)$	Hybrid characteristic	A_{ij} is the incremented surface area due to surface roughness

Table 3 Thickness and roughness parameters calculated for representative tensile coupon models

	t_{\min} (mm)	t_{\max} (mm)	t_{mean} (mm)	t_{loss} (mm)	t_{std} (mm)	COV	Sa (mm)	Sz (mm)	Sdq	Sdr (%)
A2-5-S1	0.110	4.64	2.35	6.65	0.942	0.401	0.580	3.58	0.312	25.6
A2-5-S2	0.140	5.70	2.47	6.53	1.24	0.501	1.00	5.40	0.684	53.0
A2-5-S3	0.170	4.75	2.92	6.08	0.737	0.252	0.522	4.14	0.429	33.5
A2-12-S1	2.10	6.76	5.77	3.23	0.584	0.101	0.374	4.63	0.390	25.7
A2-12-S2	3.60	6.83	5.85	3.15	0.426	0.0728	0.302	3.07	0.275	22.4
A2-12-S4	3.09	6.18	5.19	3.81	0.477	0.0919	0.355	3.27	0.351	29.0
A4-1-S1	2.44	5.71	4.71	4.29	0.584	0.124	0.355	3.06	0.291	23.4
A4-1-S2	1.88	5.77	4.59	4.41	0.557	0.121	0.389	3.55	0.335	26.8
A6-1-S3	0.760	5.03	3.76	5.24	0.646	0.172	0.453	4.00	0.427	33.0
A6-1-S4	0.570	4.73	3.44	5.56	0.632	0.184	0.437	3.67	0.409	32.5
A9-5-S1	7.97	9.07	8.61	0.394	0.160	0.0186	0.122	1.06	0.129	11.1
A9-5-S2	8.18	9.01	8.69	0.307	0.131	0.0151	0.102	0.759	0.111	9.65
A9-5-S4	5.63	8.92	8.62	0.379	0.158	0.0183	0.105	3.29	0.140	10.2
A10-1-S1	5.70	7.38	6.73	2.27	0.282	0.0419	0.211	1.75	0.220	18.2

4.2 Load-displacement characteristics

Fifty-two coupon models were analyzed. Representative load-displacement curves are plotted in Fig. 5. The scope of the current study was to investigate ductility characteristics within the zone of uniform plastic deformation, i.e. up to the maximum load. Therefore, the curves in Fig. 5 are curtailed at an elongation of 10% (5 mm), where it can clearly be seen that all the specimens have elongated beyond the point of the maximum load. The control coupon model, where there is no thickness loss due to corrosion, is also included in Fig. 5.

Fig.6 shows a replot of load-displacement curves zoomed to reveal the behaviour at yield. Corrosion-free control model exhibits a clearly defined yield point and a yield plateau. With progress in corrosion, yield point becomes obscure, which has been reported in a number of past researches. It is obvious that when corrosion is modelled by reducing thickness uniformly, yielding plateau would still be observed. Therefore, it can be deduced that the loss of yielding plateau is attributable to the unevenness of the surface.

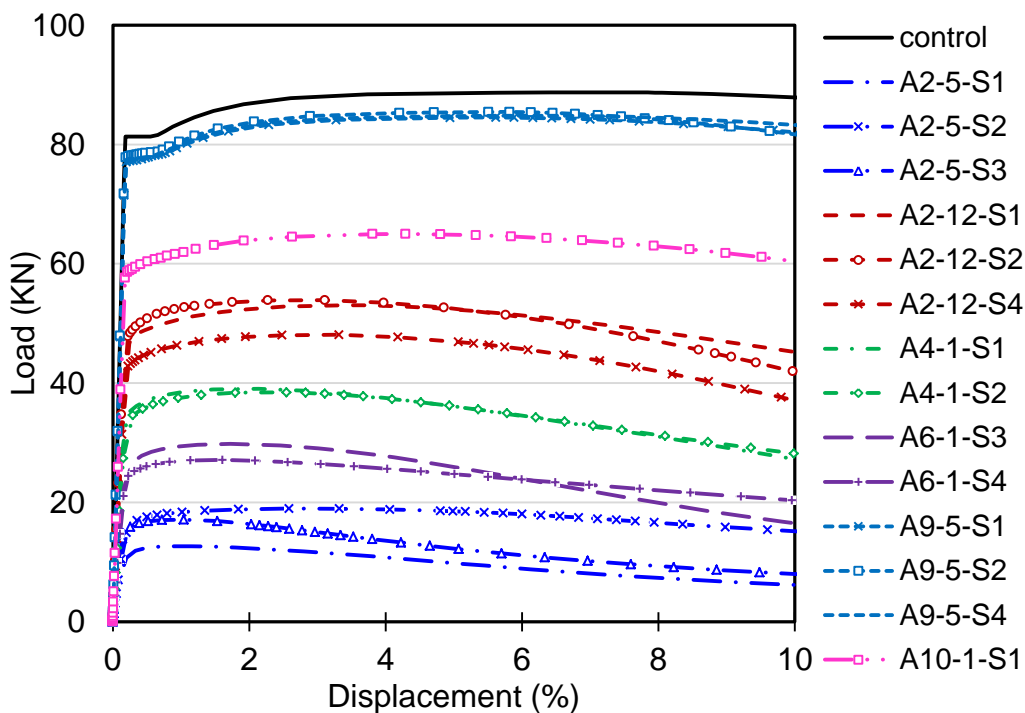


Fig. 5 Typical Load-displacement curves for the tested models

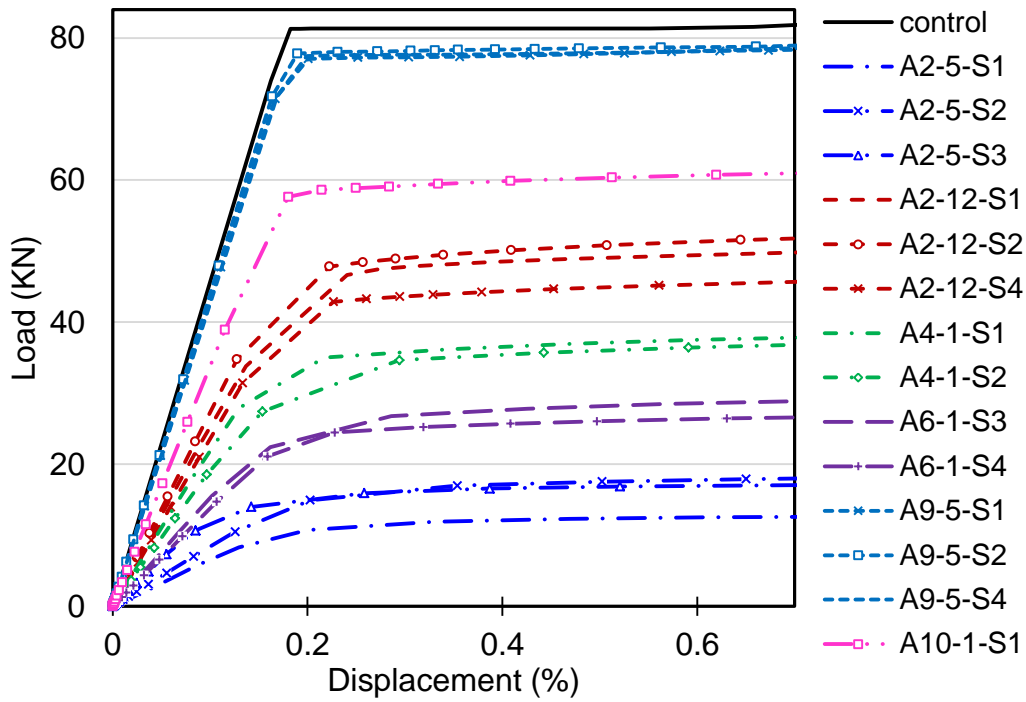


Fig. 6 Load-displacement curves for the tested models showing behaviour at yield

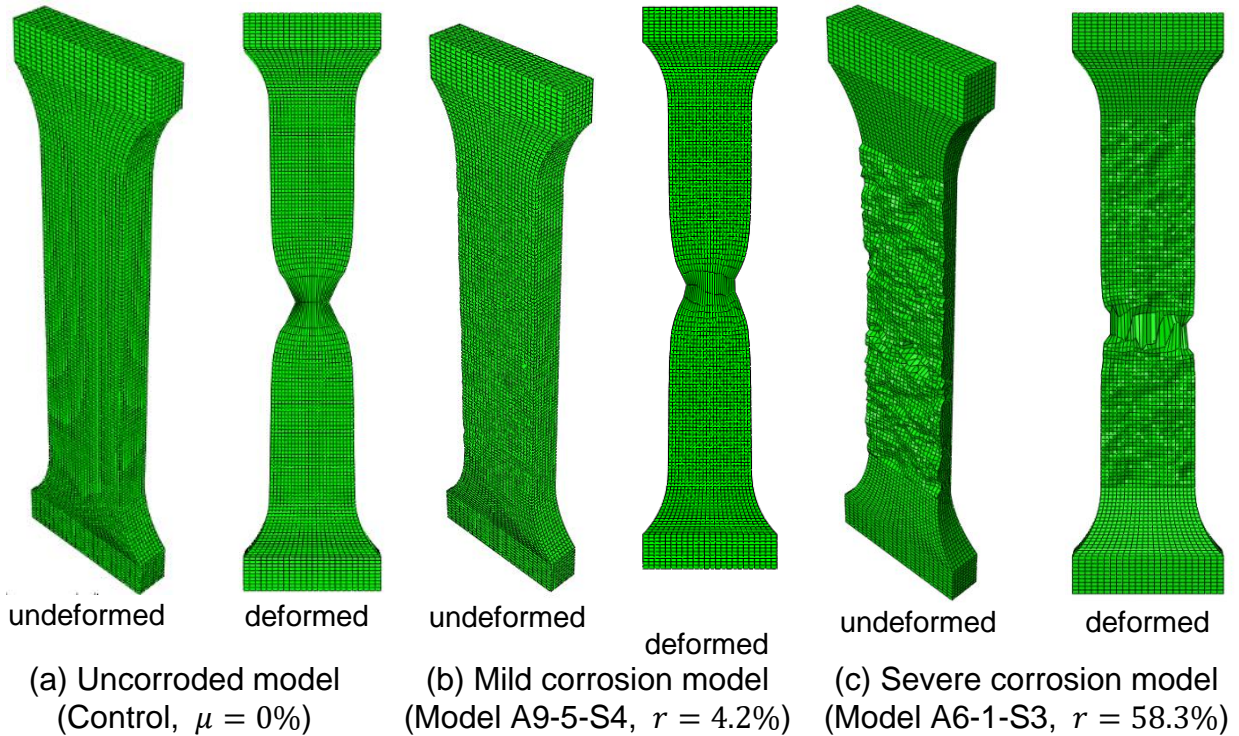


Fig. 7 Deformed shapes for different coupon models

Typical undeformed shapes and deformed shapes after the maximum load for uncorroded, mildly corroded and severely corroded coupon models are shown in Fig. 7. The classification on the degree of corrosion was used for convenience in the following discussion. The degree of corrosion, r (%), is defined as average thickness loss expressed by a percentage of the initial thickness of the specimen. In this study, for mild corrosion, $r < 50\%$, otherwise a model is classified as severe corrosion. By observation, the severely corroded model exhibits a rougher surface in comparison to the mild corrosion model.

4.3 Influence of surface roughness on ductility

Ductility is usually expressed as percent elongation or percent area reduction from a tensile test. In this paper, ductility is defined as a ratio of displacement at maximum load, δ_m , or at the failure, δ_u , to displacement at yield, δ_y , resulting into two types of ductility indices, namely, uniform plastic ductility, δ_m/δ_y , and total plastic ductility, δ_u/δ_y . In the current study, uniform plastic ductility was investigated where δ_y was taken as the elongation at yield of the uncorroded specimen. In the following discussion, the calculated ductility values were normalized by the ductility value of the uncorroded control model which is 41.8.

Although not among the ISO specified parameters, COV of remaining thickness was included in this study for purpose of comparing with previous related research. A plot of the variation of ductility with COV is shown in Fig. 8. The empirical equation proposed by Kariya (2005) is also included in this plot. It can be seen that the data from this study follow the trend of the empirical equation although the equation predicts the lower bound of the data. The trend is such that ductility decreases sharply with COV of remaining thickness and that the rate of ductility decrease becomes significantly reduced as COV increases. However, the magnitude of ductility in the current research is higher compared to the previous researcher's results. Kariya's study used corroded specimens from steel bridge girder whose material properties were close to SS 400

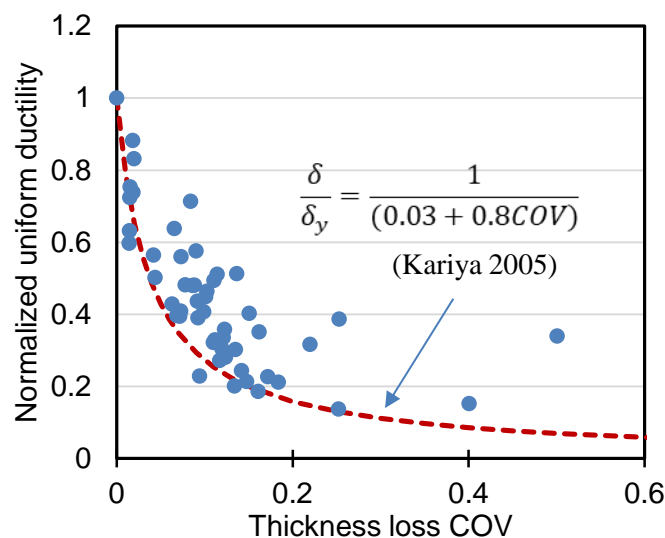


Fig. 8 Variation of ductility with COV of remaining thickness

steel. The material property is very different with the properties of SKK 490 steel considered here. While detailed investigation considering different material properties on the ductility of corroded steel is necessary to substantiate this claim, for purposes of this study, the conclusion as stated suffices.

Fig. 9 shows variation of ductility with increasing surface height characteristics. Fig. 9 (a) considers the maximum value between the highest peak and the lowest valley in the surface, S_z , while Fig. 9 (b) uses the average surface height, S_a , which captures surface roughness in the average sense. Figure 10 shows the variation of hybrid parameters, S_{dr} and S_{dq} , with ductility. These parameters combine the height and spacing characteristics of the surface roughness. As can be seen clearly in Figs. 9 and 10, ductility decreases as roughness parameter increases. An increase in the magnitude of height and hybrid parameters is an indication of increasing surface

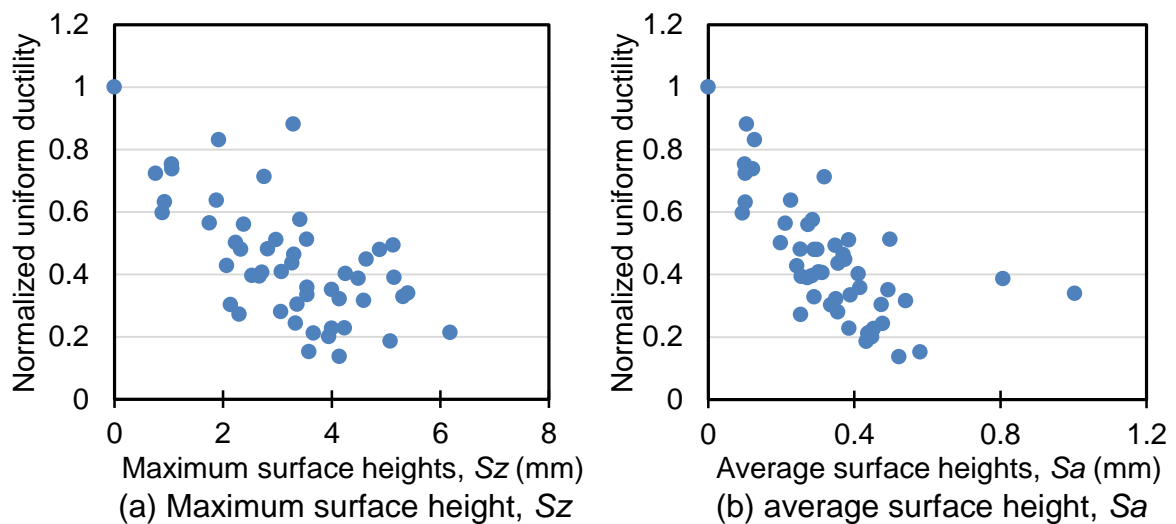


Fig. 9 Variation of ductility with surface heights characteristics

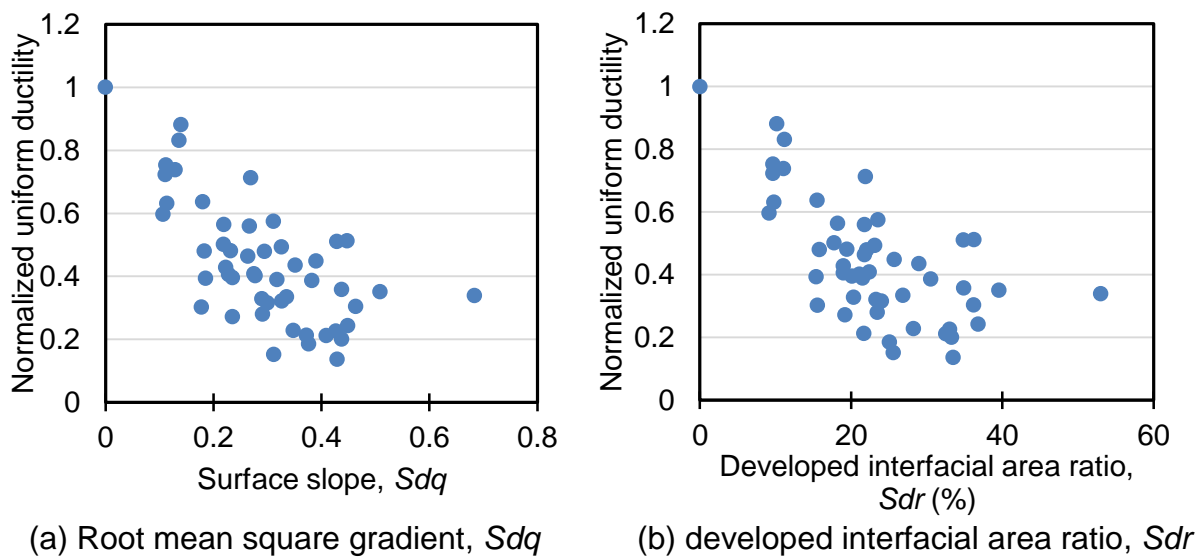


Fig. 10 Variation of ductility with hybrid characteristics

roughness.

The cause for ductility decrease was investigated by examining the deformation characteristics during loading. Equivalent plastic strain, $\bar{\epsilon}_p$, a scalar quantity that gives a measure of plastic strain was employed in this study. The distribution of $\bar{\epsilon}_p$ at different levels of loading is plotted in Figs. 11, 12 and 13, for the three categories of corrosion defined in Section 4.2. Two stages of loading are considered as follows: (a) the initiation of plastic stage just after yielding point, (b) the non-uniform plastic stage at the maximum load. In these figure, only the gauge length part of the model is shown since it is the region of interest for the determination of ductility.

For the control model, the equivalent plastic strain varies from 0% to 0.01% and from 6.0% to 7.9% at stages (a) and (b), respectively. From these calculated values as well as from the pictorial representation in Fig. 11, the variation of plastic strain distribution within the gauge length can be considered to be insignificant, and thus a conclusion can be drawn that elongation up to the maximum load is uniform for the control model as expected. In the case of mild and severe corrosion, the equivalent plastic strain varies from 0% to 0.2% and from 0% to 0.1% respectively at stage (a) and from 0% to 19.0% and from 0% to 54.4% respectively at stage (b). As can be seen in Figs. 12 and 13, manifestation of plastic strain concentration is experienced immediately after yielding with severely corroded model exhibiting the greater strain concentration than the mild corrosion model. Also strain is more localized for severely corroded model in comparison to the mildly corroded model. When strain localization occurs, the ductility of a member may be reduced, resulting in an early failure of such a member.

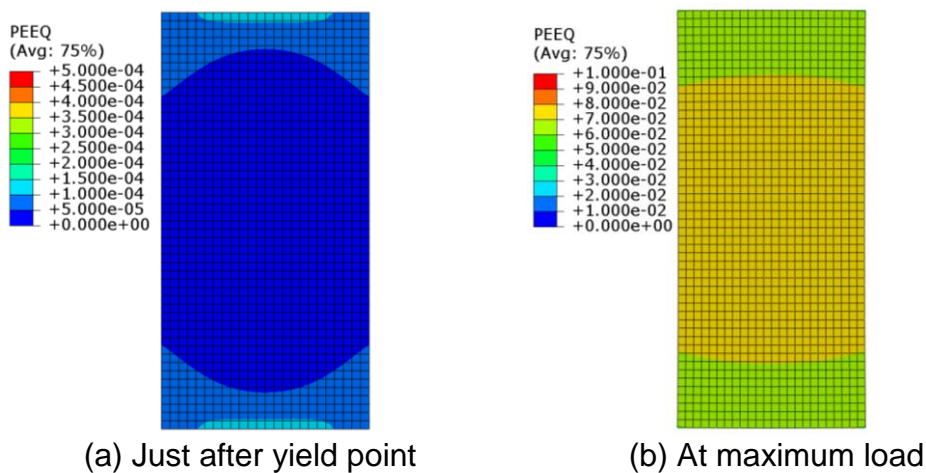


Fig. 11. Equivalent plastic strain distribution at different loading stages for control model

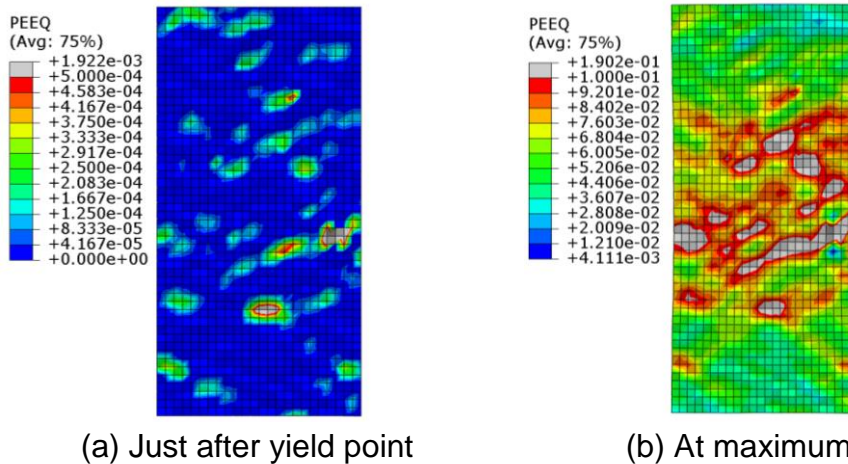


Fig. 12. Equivalent plastic strain distribution at different loading stages for mild corrosion model A9-5-S4

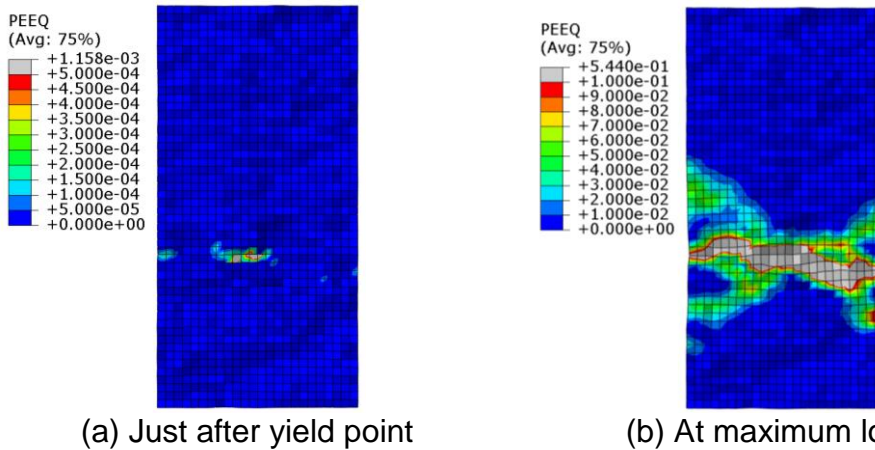


Fig. 13. Equivalent plastic strain distribution at different loading stages for severe corrosion model A6-1-S3

5. CONCLUSIONS

Numerical analyses of tensile coupons with corrosion using thickness data obtained from corroded steel pipe piles, which had been exposed to the marine environment for 19.5 years, have been conducted in this study to examine the effect of corroded surface profile on the ductility. In addition, different surface roughness parameters of the corroded coupons were determined as specified in ISO 25178-2. The relationships between the surface roughness characteristics and ductility have been investigated.

The findings from this research can be summarized as follows:

- (1) Surface unevenness due to corrosion was found to cause stress concentration and strain localization during load application. This translates to an early necking initiation in corroded steel, resulting in reduced ductility.
- (2) Ductility decreases with COV of remaining thickness. Although ductility decreases sharply when the COV of remaining thickness increases from zero, the rate

of ductility decrease is significantly reduced as COV becomes larger.

(3) In general, based on the trend from surface height and hybrid parameters, ductility decreases with an increase in surface roughness

The individual contribution of ductility decrease by the remaining cross-sectional area and surface roughness needs to be clarified in future studies.

REFERENCES

- Ahmmad, M. M., and Sumi, Y. (2010), "Strength and deformability of corroded steel plates under quasi-static tensile load," *Journal of Marine Science and Technology*, 15(1), 1–15.
- Garbatov, Y., Guedes Soares, C., Parunov, J., and Kodvanj, J. (2014), "Tensile strength assessment of corroded small scale specimens," *Corrosion Science*, 85, 296–303.
- ISO 25178 part 2 (2012), Geometrical product specification (GPS)—Surface texture: Areal— part 2: Terms, definitions and surface texture parameters. International Organization for Standardization.
- JIS Z 2241:2011 (E) Metallic materials - Tensile testing - Method of test at room temperature. Japan Industrial Standard.
- JSCE. Japan Society of Civil Engineers, Structural Engineering Committee (2009), Durability-load performance evaluation guidelines of steel structures in the marine environment, Structural Engineering series 19, the Japan Society of Civil Engineers (in Japanese).
- Kariya, A., Tagaya, K., Kaita, T., and Fujii, K. (2005), "Mechanical Strength of Corroded Plates Under Tensile Force," *Collaboration and Harmonization in Creative Systems - Hara (Ed.)*, Taylor and Francis Group, 105-110.
- Mathworks. (2018), MatLab version R2018a. Natick, Massachusetts. *The MathWorks Inc.*
- Qin, G., Xu, S., Yao, D., and Zhang, Z. (2016), "Study on the degradation of mechanical properties of corroded steel plates based on surface topography," *Journal of Constructional Steel Research*, 125, 205-217.
- Simulia, (2014). Abaqus 6.14 English documentation. *Dassault Systèmes, Providence, RI, USA.*
- Suzuki, Y., Akamine, K., Kanesaka, K., and Imazeki, M., (2008), "Development of New Anti-Corrosion Method (IECOS) for Marine Steel Structures," *IHI Engineering Review*, 41(2), 58-67.
- Tamura, I., Watanabe, E., Itoh, Y., Fujii, K., Nogami, K., Sugiura, K., Nagata, K. and Oka, T. (2005) "Remaining Structural Performance of Steel Pipes Corroded in Marine Environment," *Journal of Structural Engineering*, 51A, 1103-1110 (in Japanese).
- Wang, L., and Tong, W. (2015), "Identification of post-necking strain hardening behavior of thin sheet metals from image-based surface strain data in uniaxial tension tests," *International Journal of Solids and Structures*, 75–76, 12–31.